



Cause identification of damage in tunnel constructed in soil-rock mixture site and effect of suggested reinforcement measures

Xiaoguang Jin^{1,2,3} · Chao Hou^{1,2} · Yayong Li⁴ · Wenjun He⁵

Received: 3 October 2020 / Accepted: 12 May 2021 / Published online: 26 May 2021
© Saudi Society for Geosciences 2021

Abstract

A running tunnel in Chongqing, China was constructed in a soil-rock mixture (SRM) by the open-cut method. During the construction period, severe cracks occurred on the tunnel lining floor, which will significantly affect the tunnel's long-term stability. In this study, the numerical investigation was performed to study the development trend of damage zones in the tunnel lining, identifying the causes of damage and further evaluating the effects of suggested reinforcement measures. Firstly, numerical modeling experiments were conducted to obtain the physical and mechanical parameters of SRM. Then, three 3-dimensional (3D) numerical simulation models were established. The settlement, tensile stress, and distribution of damage zones on the tunnel floor were highlighted. Results indicated that the maximum deformation occurs on the roof of the tunnel lining, and the minimum displacement is in the middle part of the tunnel floor. The maximum compressive stress is within the ultimate compressive strength. However, the tensile strength significantly exceeded the ultimate tensile strength, resulting in cracks in the tunnel lining. If no reinforcement measures are taken, about 66% of the tunnel floor will be tensioned to damage, significantly reducing the bearing capacity and long-term stability of tunnel lining. The stiffness difference between SRM and the bored piles is the reason for damage zones in tunnel lining. It is suggested that grouting reinforcement and steel fiber reinforced concrete should be taken on the tunnel floor to improve damage resistance. Finally, it is verified that the suggested reinforcement measures can effectively control uneven settlement and damage zones in the tunnel floor.

Keywords Damage zone · Soil-rock mixture · Uneven settlement · Stress distribution · Reinforcement measures · Numeric simulation

Responsible Editor: Zeynal Abiddin Erguler

✉ Xiaoguang Jin
jinxiaoguang@cqu.edu.cn

¹ School of Civil Engineering, Chongqing University, Chongqing 400045, China

² Key Laboratory of New Technology for Construction of Cities in Mountain Area of the Ministry of Education, Chongqing University, Chongqing 400045, China

³ State Key Laboratory of Coal Mine Disaster Dynamics and Control, Chongqing University, Chongqing 400045, China

⁴ China Construction Tunnel Co., Ltd., Chongqing 401320, China

⁵ South City Power Supply Branch of State Grid Chongqing Electric Power Company, Chongqing 404100, China

Introduction

Soil-rock mixture (SRM) is a complicated material widely encountered in geotechnical engineering projects (Xu et al. 2007). The physical and mechanical properties of SRM are quite different from soil or rock. Some researchers have devoted themselves to investigating the physical and mechanical properties of SRM by laboratory and in-situ experiments (Vallejo and Mawby 2000; Li et al. 2004; Xu et al. 2008; Xu et al. 2011). However, the laboratory and in-situ tests have the disadvantage of only representing the local region's mechanical characteristics, which may significantly affect the accuracy of calculation results. With the rapid development of the finite element method (FEM), the mechanical properties and failure characteristics of SRM have been investigated by some scholars through numeric modeling experiments (Yue et al. 2003; Xu et al. 2008; Fakhimi 2009). For instance, Sun (2014) carried out numeric experiments to obtain the shear strength parameters of SRM through Finite Difference

Software Flac3D. Results show that the mechanical parameters of SRM obtained through Flac3D are almost identical to the direct in-situ test results. It has been widely accepted that FEM is effective in obtaining mechanical parameters of SRM.

Chongqing is a city in the southwestern part of China that is famous as a mountain city. Over the past several decades, many small mountains were blasted to construct buildings in Chongqing. The rock and soil produced by the blasting were mixed and randomly abandoned in gullies. Nowadays, with the rapid development of Chongqing, subways were constructed to solve traffic jams. However, the transportation system's space was limited; therefore, many subways were designed to be built in SRM. For example, the running tunnel between the Jiangbeicheng and Wulidian subway stations was constructed in SRM at the beginning of 2008. During the construction period, severe longitudinal cracks occurred on the floor of the tunnel lining. Based on engineering experiences, the tunnel lining cracks will decrease the effective bearing area, further reducing the tunnel's long-term stability. Besides, groundwater can penetrate the tunnel through cracks and then influences traffic safety.

Some scholars have devoted themselves to studying the causes of tunnel lining damage, cracking mechanisms, and reasonable reinforcement measures (Richards 1998; Lee et al. 2013; Wang et al. 2014). For instance, Wang (2010) presented the possible causes of lining anomalies by systematically studying the spatial distributions, textures, and appearances of cracks on a tunnel lining surface. Xiao (2014) conducted a 3D numeric modeling to simulate tunnel construction and analyze the cracking mechanism in the secondary lining. Some scholars have adopted several reinforcement measures (Mashimo et al. 2006; Chiaia et al. 2009) to repair the damage zones in the tunnel lining and ensure the long-term stability of the tunnel. The steel fiber-reinforced concrete has been validated to be an effective way to control damage development. Mashimo (2006) studied fiber-reinforced concrete's effect on preventing cracks in tunnel lining by comparing plain concrete and steel fiber-reinforced concrete. Chiaia (2009) examined the effect of steel fiber in reinforced concrete on improving tensile strength and controlling crack width in tunnel linings. The proposed approach has been successfully applied to the design of tunnel linings in Italy.

The literature review results showed that most of the studies were focused on the physical and mechanical properties of SRM, cracking mechanisms of tunnel lining, and reasonable reinforcement measures. However, little attention has been paid to identifying the causes of damage zones in a tunnel constructed in SRM and evaluating the effectiveness of corresponding reinforcement measures. In this paper, the numerical simulation was conducted to investigate the settlement, tensile stress, and distribution of damage zones on the tunnel floor. Besides, the causes of the cracks in the tunnel floor were identified. Then, the effects of the two reinforcement measures were verified. Finally, some suggestions were forwarded for

similar engineering projects in the future. The theme of this work is to offer a theoretical basis for the construction and disease control of similar projects.

Materials and methods

The running tunnel between the Jiangbeicheng and Wulidian subway stations is a part of metro line 6 in Chongqing, China. It was constructed at the beginning of 2008. The buried depth of the running tunnel is approximately 15 m. The total length is about 320 m. According to the design document, this tunnel was constructed in SRM by the open-cut method. The geological profile of the tunnel site area is shown in Fig. 1. It should be noted that Q_4^{ml} represents SRM, and that J2s-Ss represents sandstone. The landscape in the tunnel site was originally a valley and was later backfilled by SRM. The elevation of the surface varies from 216 m to 223 m. In the central part of the engineering site, the surface is not flat, with the slope angle ranging from 5 to 15°.

Manual bored piles were designed to decrease settlement in the tunnel floor to ensure the tunnel's stability (Fig. 1). The boring piles' designed diameter is 1.5 m, with the center to center spacing of 5 m. The bottom of bored piles was embedded in moderately weathered sandstone. In engineering practice, the tunnel's construction steps are as follows: SRM in the tunnel site was excavated to the designed elevation. Then, bored piles were constructed. Tunnel lining was cast in situ after the bored piles were completed. After the curing period of concrete, the tunnel was covered through backfilling SRM above the tunnel. The thickness of the backfill above the tunnel lining varies from 7 m to 14.8 m.

Generally, tunnel lining cracks are divided into three types: longitudinal, circumferential, and oblique. When the cracks of the tunnel structure are parallel or substantially parallel to the axial direction of the tunnel, they are called longitudinal cracks. This kind of crack is the most harmful type of crack because it destroys the integrity of the lining section. In double-track tunnels, longitudinal cracks are mainly produced in the arch waist and shoulders, while in single-track tunnels, the longitudinal cracks are mainly produced in the floors and sidewalls. When the geological conditions are biased, the

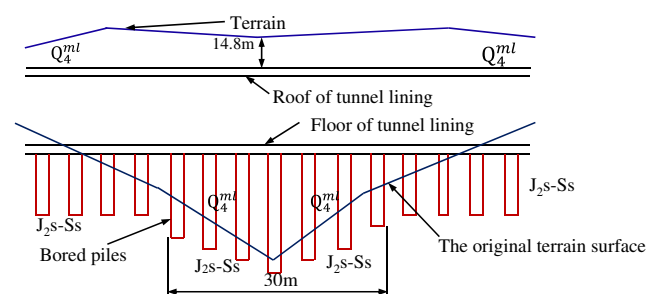


Fig. 1 Geological profile in tunnel site

tunnel produces uneven settlement, the tunnel is under-excavated during construction, or the top of the middle wall is not entirely backfilled, longitudinal cracks in the tunnel lining are likely to occur. According to the construction records, many longitudinal cracks occurred on the tunnel lining floor when backfilling to 9 m above the tunnel (Fig. 2). The depth and width of the cracks were detected through geological radar. As a result, the cracks' width varies from 0.2 to 0.3 mm, and the depth ranges from 1.4 to 3.5 cm. Besides, the distribution of the cracks is mainly along the middle line of the tunnel floor, as depicted in Fig. 2(b).

Reinforcement measures

Generally, damage zones in the tunnel lining were commonly dealt with in two ways. On the one hand, the sleeve grouting method and bolt anchorage method can be adopted to decrease the stiffness difference between SRM and bored piles, further decreasing uneven settlement and improving stress distribution. On the other hand, tunnel lining's damage resistance can be improved by replacing concrete with steel fiber-reinforced concrete. Another reinforcement measure, such as adding a new reinforced concrete arch in the existing tunnel lining, constructing a support beam in the bottom of the tunnel lining, can also be taken to deal with damage zones in tunnel lining. Nevertheless, the above two methods were not feasible since the tunnel clearance limit should be guaranteed, and the tunnel lining has been covered when damage cracks were found. It is suggested that the sleeve grouting method and the steel fiber-reinforced concrete method can be taken in engineering practice. These two adopted reinforcement measures are described in detail in the following part.

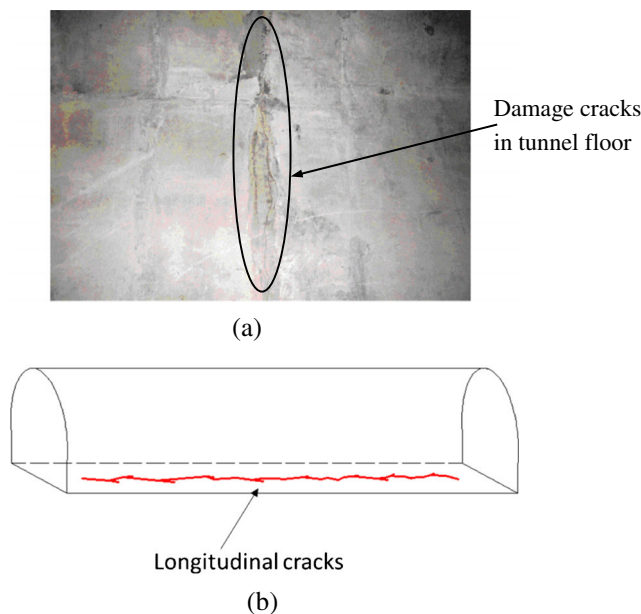


Fig. 2 Damage cracks in the floor of tunnel lining. (a) Pictures of the project. (b) Diagram of the longitudinal cracks in the tunnel floor

Steel fiber-reinforced concrete method

It has been validated that steel fiber-reinforced concrete can significantly increase the tensile strength and damage resistance (Mashimo et al. 2006; Chiaia et al. 2009). In this method, the damaged concrete in the tunnel lining was excavated and replaced by steel fiber-reinforced concrete. The thickness of the fiber-reinforced concrete was approximately 0.4 m. The concrete on the tunnel floor's surface was cut anomalously to improve the fresh and old concrete's adhesive properties. The tensile strength of steel fiber-reinforced concrete can be calculated using Eqs. (1) and (2) that are stipulated by the *Technical specification for fiber reinforced concrete structures* (Dalian University of Technology, 2004).

$$f_{fjk} = f_{tk} (1 + \alpha_t \lambda_f) \tag{1}$$

$$\lambda_f = \rho_f l_f / d_f \tag{2}$$

where: f_{fjk} is the characteristic value of the tensile strength of the fiber-reinforced concrete, with the unit of MPa; f_{tk} is the characteristic value of the tensile strength of the C40 concrete, with the unit of MPa; λ_f is the characteristic value of the fiber content; ρ_f is the volume fraction of the steel fiber; l_f is the length of the steel fiber, with the unit of mm; d_f is the equivalent diameter of the steel fiber, with the unit of mm; α_t is the influence coefficient of the steel fiber on the tensile strength of the fiber-reinforced concrete.

Sleeve grouting method

Generally, cement grouting bonds the soil and the rock in SRM. Thus, the elastic modulus and shear strength increase significantly, resulting in the decrease of uneven settlement and tensile stress on the tunnel floor. In engineering practice, cement grouting is injected into the pores in the SRM through grouting holes drilled in the tunnel floor.

Physical and mechanical parameters of SRM

Through field investigation, the distribution of SRM in the tunnel site was depicted in Fig. 3. It can be found that rocks are angular and are distributed randomly. The size of the rocks varies from 0.2 to 0.5 m. It is widely accepted that



Fig. 3 Investigational area of SRM in tunnel site

Table 1 The percentages of the original and after allocation of gravel fraction

Particle size(cm)	Less than 2	2–10	10–18	18–26	26–34	34–42	42–50	More than 50
Percentage content	9%	17%	21%	15%	10%	11%	8%	9%
Percentage content after treatment	—	18.5%	22.5%	16.5%	11.5%	12.5%	9.5%	—

geotechnical materials' mechanical properties play a crucial role in the failure characteristics of geotechnical engineering. The physical and mechanical properties of the SRM in the tunnel site should be obtained first to identify the causes of tunnel lining cracking. In engineering practice, cracks were found when backfilling to 9 m above the tunnel, which means that there is no enough testing site to conduct an in-situ direct shear test. Besides, the size of rocks in the tunnel site is too large to conduct laboratory tests. In this paper, the numeric modeling experiments were adopted to obtain physical and mechanical parameters of SRM.

The particle size distribution of SRM was determined through the sieving method stipulated by *Test Methods of Soils for Highway Engineering* (Research Institute of Highway Ministry of Transport, 2007). The sieving method results show that the rock content of the soil-rock mixture is 60%. When establishing the numeric model, if the particle size is less than 2 cm, it will be ignored. If the particle size is more than 50 cm, it will be evenly distributed to other particle groups according to the equivalent substitution method. The original statistical percentage content of each particle group and the percentage content after distribution according to the above principles are shown in Table 1.

It is assumed that the particle size distribution in each particle group obeys uniform distribution. According to the proportion of each particle group in the total gravel area and the selected gravel particle size, the number of gravel with each particle size shall be allocated to conform to the original percentage content of the gravel particle group in Table 1 as far as possible.

Two numeric models that can truly reflect the spatial distribution of SRM were established by using the Rand command in MATLAB and imported into finite element software. Figure 4 noted that the rectangle represents rock, and the other part represents soil. The numeric model size was selected as 3 m (six times the maximum size of rocks) to reduce the effect of boundary conditions on numeric results. Soil and rocks in numeric models belong to two different groups. The physical and mechanical parameters of soil and rock were introduced into corresponding groups. According to the geological survey report, the physical and mechanical parameters of soil and rock in the tunnel site are listed in Table 2.

Numeric modeling experiments were conducted under three different confining pressures 0, 0.5, and 1.0 MPa. The confining pressure was applied on the horizontal surface of the numeric model. The displacement load method was used to apply vertical load on the top of the numerical model with 1e-6m/step. Rigid constraints are applied to the bottom of the numerical model. The stress and strain of the characteristic points in the numerical model are recorded during the loading process.

The effectiveness of the numeric modeling experiment was validated by comparing computational results to the physical and mechanical parameters in the geological survey report. Based on the numerical simulation results of homogeneous rock mass, the friction angle of the rock is 35.84° , the cohesion is 1225.2 KPa, the elastic modulus is 1965 MPa, and the Poisson's ratio is 0.327. Comparing the mechanical parameters of the rock in Table 2, it can be seen that the error is relatively minor.

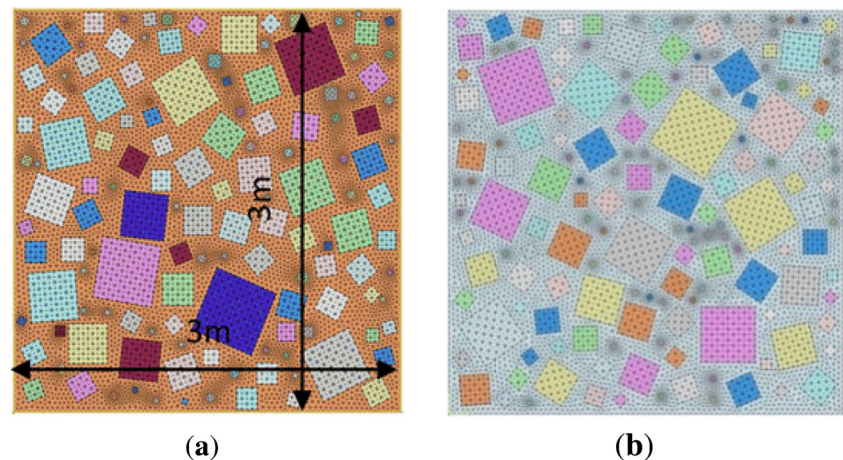
Fig. 4 Numeric models of SRM. (a) Model I, (b) Model II

Table 2 Physical and mechanical parameters of soil and rock

Type	Density/ (kg/m ³)	Elastic modulus/MPa	Cohesion/ kPa	Internal friction angle/(°)	Poisson’s ratio	Tensile strength/kPa
Soil	2000	20	40.0	28	0.42	9.0
Rock	2570	1965	1029	40	0.32	575

To further validate the effectiveness of numerical simulation, the trend of the stress-strain curve obtained from numerical simulation and laboratory tests was compared. Zhao and Liu (2019) carried out a medium triaxial experiment for SRM and obtained the stress-strain curve of SRM with different rock content (0, 10, 30, 50, and 70%). The test device and results are depicted in Fig. 5; the stress-strain curve can be divided into three stages: (1) linearly stage: at this stage, the stress increases approximate linearly with the strain; (2) strain hardening stage: at this stage, the stress increases continuously with strain, but the increased range is small. (3) Steady stage: at this stage, the stress increases little with strain and tends to be stable. Compared with the stress-strain curve of SRM acquired from the numerical simulation (Fig. 6), we can see that the curve also can be divided into three stages (i.e., linearly stage, strain hardening stage, and steady stage). The evolution trend of the stress-strain curve in Fig. 5 (laboratory test) and Fig. 6 (numerical simulation) is the same. Combined with the fact that there is a minor error in the mechanical parameters of rock between the test data (geological survey report) and the numerical simulation. We can deduce that it is practical to apply this method to obtain the mechanical parameters of the SRM.

Figure 6 shows curves of axial stress versus the axial strain of the two models. The ultimate compressive strength increases with the increase of confining pressure. The ultimate compressive strength of SRM was much larger than that of soil, which means that rocks in SRM can significantly

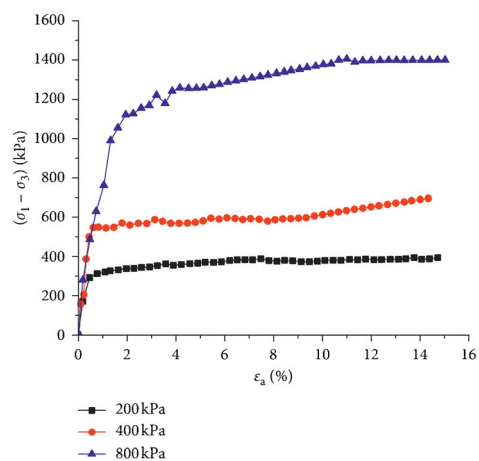
improve the mechanical strength of the soil. Fig. 7 shows the failure mode of soil and SRM samples, respectively. Note that the green color represents zones that were in a plastic state. X type shear failure occurred in the soil sample, while the failure mode of SRM was quite different. In the SRM sample, most of the soil elements yielded, but only a few rock elements yielded. Plastic zones in soil elements bypass rock elements and are finally connected. The failure model of SRM was similar to the laboratory results of Wang’s study (Wang et al. 2014).

The Mohr-Coulomb yield criterion was used to calculate the mechanical parameters of SRM. The mean value of these two models was selected as the comprehensive mechanical parameters of SRM. The internal angle friction is 32.75°, and the cohesion is 171.67 kPa. The elastic modulus of SRM is calculated according to the stress-strain curves when the confining pressure is 0 MPa. The elastic modulus can be calculated to be 203 MPa.

In engineering practice, the grouting holes’ depth varies from 4 to 5 m, with an interval of 1.5 m. The physical and mechanical parameters of SRM before and after grouting are listed in Table 3. It is worth noting that the mechanical parameters of SRM before grouting were obtained from the numerical simulation results in the “Physical and mechanical parameters of SRM” section. After grouting, the mechanical parameters of SRM are obtained by statistics of relevant literature data (Wang 2009; Zhang 2010; Cui 2012).



(a)



(b)

Fig. 5 Test device and results of the triaxial experiment for SRM (Zhao and Liu 2019). (a) Medium triaxial test system. (b) Stress-strain curve of SRM with a 50% rock content

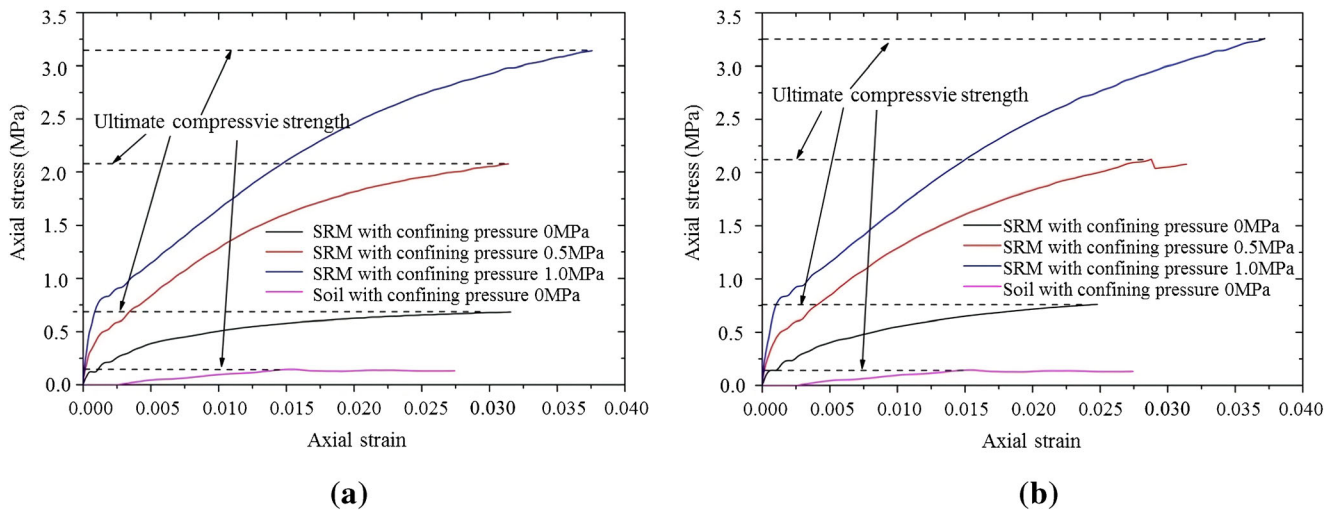


Fig. 6 The curve of axial stress versus axial strain. (a) Model I, (b) Model II

Development trends and causes of damage zones

After the curing period of concrete, SRM was backfilled to cover the tunnel. Damage zones in tunnel lining were found when backfilling to 9 m. The loading pressure acting on the tunnel lining should be accurately calculated to identify the development trends and causes of damage zones in the tunnel lining. The *Code for Design of Road Tunnel* (China Merchants Chongqing Communications Technology Research & Design Institute CO., LTD. 2010) introduces two calculation methods: the load-structure method and the layer-structure method, to calculate the loading pressure applied to the tunnel lining. The load-structure method has the disadvantages that it ignores the self-bearing capacity of SRM, which will magnify the loading pressure acting on tunnel lining than actual. In this study, the layer-structure method was selected to calculate the deformation and stress distribution in the tunnel lining. A comprehensive 3D numeric model was established by Midas-GTS, which is widely used in geotechnical engineering. It was selected to conduct numeric simulation since it can competently deal with the discontinuous

deformation problem and solve the slip problem between SRM and tunnel lining.

Numeric modeling

Severe damage occurred in the center 30 m of the tunnel shown in Fig. 1. This part is selected to establish the 3D numeric model (Fig. 8). The dimensions of the built model are $50 \times 30 \times 54.8 \text{ m}^3$, with a buried of 14.8 m. The backfill above the tunnel lining was divided into two parts according to construction progress. The height of the lower part is 9 m, and the height of the upper part is 5.8 m. Rock masses, tunnel lining, grouting reinforcement, fiber-reinforced concrete, and bored piles were meshed using the tetrahedron element. In total, it was composed of about 130,235 elements and 22,625 grid points. The boundary conditions are set as follows: nodes at all sides of the model were fixed in the horizontal direction on the x-z and y-z planes (i.e., $x = -25$, $x = 25$, $y = 0$, and $y = 30$). Nodes at the base of the model ($z = 0$) were fixed in the vertical (z) direction, and nodes on the top of numerical models are free. In order to simulate the slip

Fig. 7 Failure model of soil and SRM sample. (a) Soil, (b) SRM

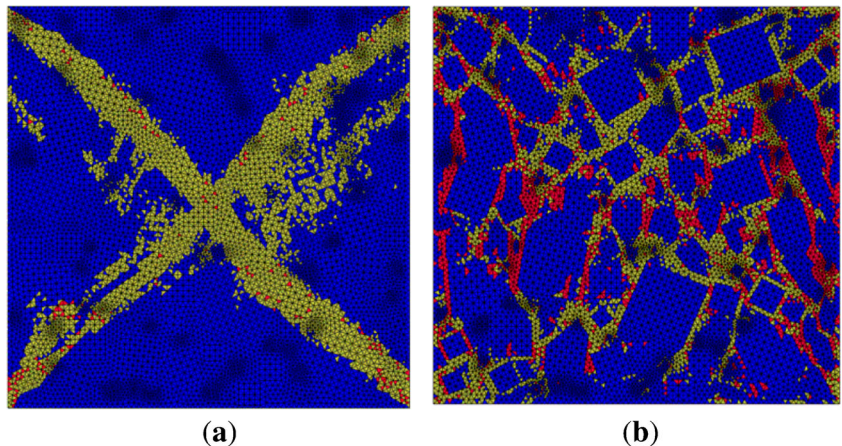


Table 3 Mechanical Parameters of SRM before and after grouting

SRM	Density/(kg/m ³)	Elastic modulus/(MPa)	Cohesion/(kPa)	Internal friction angle/(°)	Poisson's ratio
Before grouting	24.38	203.00	171.67	32.75	0.369
After grouting	25.36	263.90	231.75	39.30	0.351
Increment	4%	30%	35%	20%	-5%

between SRM and tunnel lining, the interface element was established in the interface between tunnel lining and SRM. The friction coefficient was selected to be 0.5 based on engineering experiences.

In engineering practice, the construction steps can be roughly divided into three construction steps. Firstly, after casting the tunnel lining, the initial stress field was generated; meanwhile, the calculated displacement was reset to be 0. Then, backfill was backfilled to 9 m above the tunnel lining. Finally, backfill was backfilled to 14.8 m above the tunnel. The numeric simulation's construction steps are consistent with that in engineering practice to investigate the causes of damage zones in the tunnel lining and evaluate the reinforcement measures' effect. Based on the three working conditions listed in Table 4, three numerical models were established. The deformation and stress distribution in tunnel lining was highlighted.

Physical and mechanical parameters used in the numeric simulation

The physical and mechanical parameters of materials in the numeric simulation are listed in Table 5. Concrete obeys the elastic model. The physical and mechanical parameters of it are selected based on existing experimental results. SRM and sandstone both obey the Mohr-Coulomb yield criterion, and the ideal elastic-plastic constitutive model is adopted in the mechanical model of SRM and sandstone. The physical and mechanical parameters of sandstone are selected according to

the geological survey report. The physical and mechanical parameters of SRM were determined by numerical modeling experiments in the "Materials and methods" section.

In engineering practice, the primary purpose of grouting is to improve the mechanical parameters of SRM. Therefore, the grouting reinforcement was simulated by changing the grouting reinforcement area's physical and mechanical parameters below the tunnel lining. Fiber-reinforced steel concrete is simulated by adding elements on the surface of the tunnel floor.

Results and analysis

Development trend of damage zones

The distribution of settlement, stress, and damage zones of model 1 in construction steps 2 and 3 was compared to investigate the development trend of damage zones in tunnel lining with the height of backfill. Fig. 9 shows the vertical displacement of the tunnel lining when backfilling to 9 and 14.8 m. The tendency of these two deformation contours was similar. The maximum deformation occurs on the roof of the tunnel lining. The minimum displacement is in the middle part of the tunnel floor. The maximum displacement increased from 10.7 to 16.4 mm when backfilling to 14.8 m compared to 9 m. Due to the supporting effect of bored piles, the minimum displacement occurred in the central part of the tunnel floor.

Fig. 8 3D numeric models. (a) The isometric view. (b) Tunnel lining, grouting reinforcement, and piles

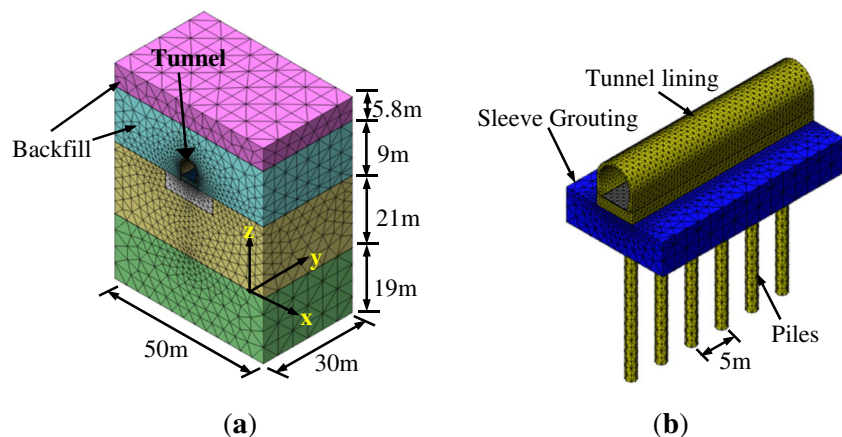


Table 4 Working conditions

Working conditions	Types of foundation	Reinforcement measures
Model 1	Upon SRM and is supported by bored piles	Without reinforcement measures
Model 2	Directly upon SRM	Without reinforcement measures
Model 3	Upon SRM and is supported by bored piles	Sleeve grouting and fiber reinforced concrete

Figure 10 shows the distribution of stress and damage zones in the tunnel lining when backfilling to 9 and 14.8 m. Noted that the positive value represents tensile stress, and the negative value represents compressive stress. Stress in the tunnel floor varied from -6.02 to 6.57 MPa when backfilling to 9 m. It can be found that the characteristic tensile strength and compressive strength of C30 concrete are 2.01 and 20.1 MPa, respectively. The maximum compressive stress is within the ultimate compressive strength. However, the tensile strength significantly exceeded the ultimate tensile strength, resulting in cracks in the tunnel lining. The area in which the corresponding tensile stress exceeds the ultimate tensile strength of concrete is defined as the damage zone. Damage zones mainly distribute in the middle part of the tunnel floor. The damage zones' width and thickness are 2.6 and 0.5 m, respectively, when backfilling to 9 m. The maximum depth of damage zones occurred in the center of the tunnel floor and gradually decreased. The width of the tunnel floor is 6.0 m. About 43.3% of the tunnel floor will be damaged. The location of the damage zones is consistent with that in the engineering practice, which validates numeric simulation's effectiveness and the correctness of the selected mechanical parameters.

Tunnel lining damage was found when backfilling to 9 m. At this time, there is still 5.8 m of backfill left to the design elevation. It is suggested that if tensile stress and damaged zones do not increase significantly when backfilling to 14.8 m, damage zones could be dealt with using a grouting agent without taking other reinforcement measures. Nevertheless, if the damage zones increase significantly, special reinforcement measures should be taken to control the development of the damage zones in the tunnel lining. Fig. 10(b) shows the

development of stress and damage zones distribution when backfilling to 14.8 m. The tensile stress and damage zones both significantly increase compared to that when backfilling to 9 m. The maximum compressive strength is still within the ultimate compressive strength of concrete, while the maximum tensile strength increased to 9.81 MPa. The width and thickness of the damage zones increased to 4.0 and 0.55 m, respectively. About 66.6% of the tunnel floor will be tensioned to damage.

It can be inferred from the above results that if no control measures were taken when backfilling to 9 m, tensile strength and damage zones would significantly increase, resulting in a severe reduction of the serviceability long-term stability of the tunnel. It is suggested that backfilling can be continued after taking reasonable reinforcement measures to control the development of damage zones in tunnel lining.

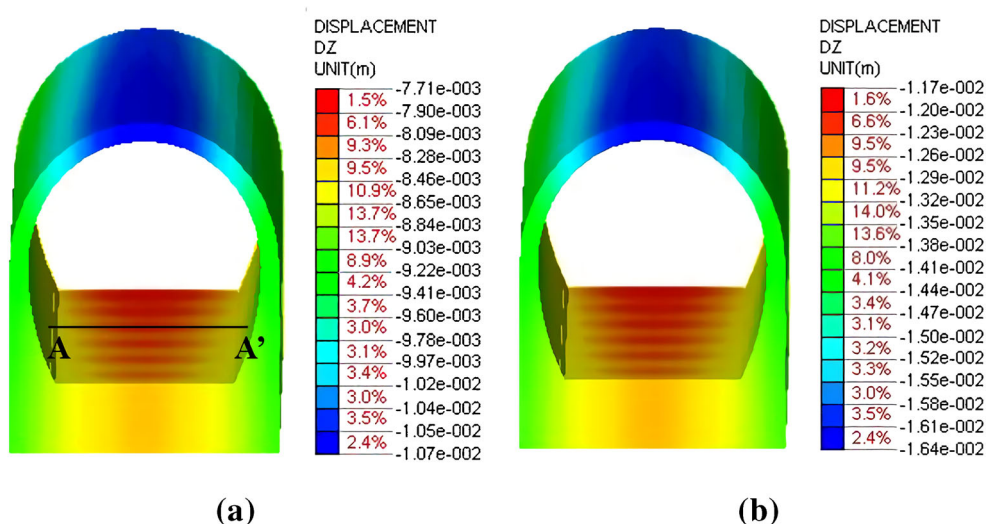
Causes of damage zones in tunnel lining

Settlement along the line B-B' (Fig. 10) of models 1 and 2 was extracted to study the settlement distribution in tunnel floor. The results are shown in Fig. 11(a). The deformation of the tunnel floor increases with the height of the backfill above the tunnel lining. Due to bored piles, the settlement of model 1 is much smaller than model 2. However, the settlement of model 1 was not identical. The settlement on the edges of the tunnel floor is larger than the central part. The maximum uneven settlement on the tunnel floor is 1.24 mm when backfilling to 9 m and increased to 2.03 mm when backfilling to 14.8 m. Settlement in model 2 is much larger than model 1, but it distributes entirely without the uneven settlement.

Table 5 Physical and mechanical parameters used in numeric simulations

Materials	Density/(kg/m ³)	Elastic modulus/(MPa)	Cohesion/(kPa)	Internal friction angle/(°)	Tensile strength/(MPa)
C30 concrete	2500	31.3			2.01
SRM before grouting	24.38	0.203	171.67	32.75	
SRM after grouting	25.36	0.264	231.75	39.30	
Sandstone	2730	4.73	1858	40.5	0.43

Fig. 9 Vertical displacements of the tunnel lining. (a) Backfilling to 9 m. (b) Backfilling to 14.8 m

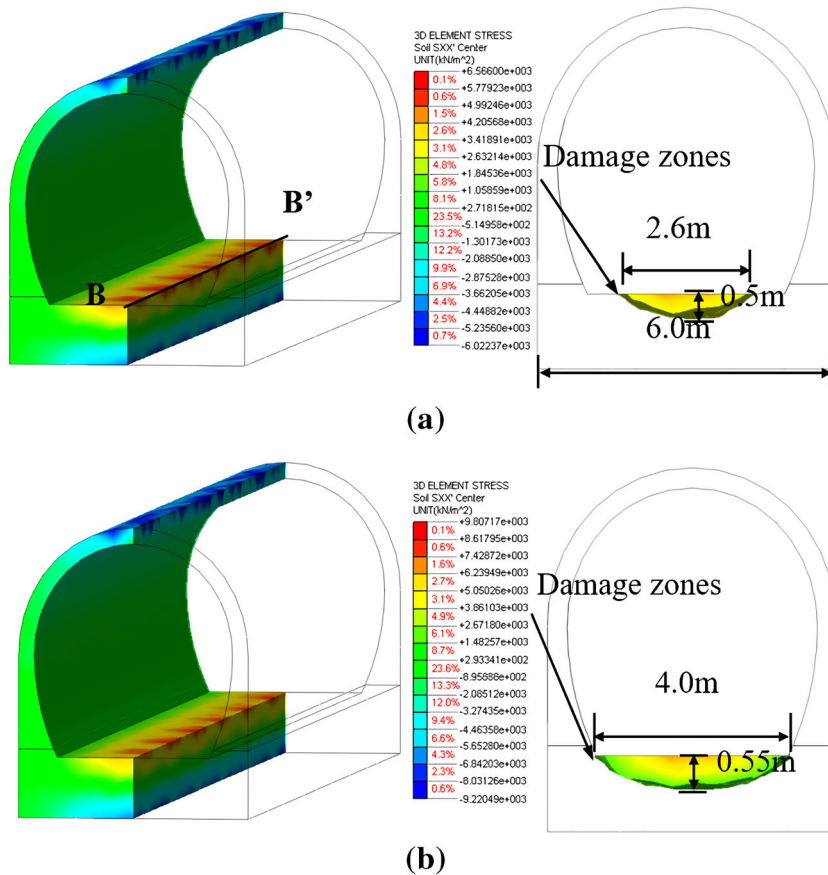


Tensile stress along line B-B' (Fig. 10) was extracted to compare the stress characteristics of models 1 and 2. Variation of tensile stress along line B-B' is depicted in Fig. 11(b). It can be seen that the tensile stress in model 1 is not uniform. Tensile stress on the tunnel floor constructed above bored piles is much larger than that above SRM. Tensile stress in model 1 ranges from 5 to 7 MPa when backfilling to 9 m. It increases from 8 to 11 MPa when backfilling to 14.8 m.

However, the maximum tensile stress in model 2 is much less than in model 1. Tensile stress distributes uniformly on the tunnel floor. The maximum tensile stress in model 2 is approximately 2 MPa, which is within the concrete's ultimate tensile strength.

To sum up, the settlement of model 1 is smaller than model 2 at the expense of significant uneven settlement. Tensile stress in model 2 is within the ultimate tensile strength of

Fig. 10 Distribution of stress and damage zones in tunnel lining. (a) Backfilling to 9 m. (b) Backfilling to 14.8 m



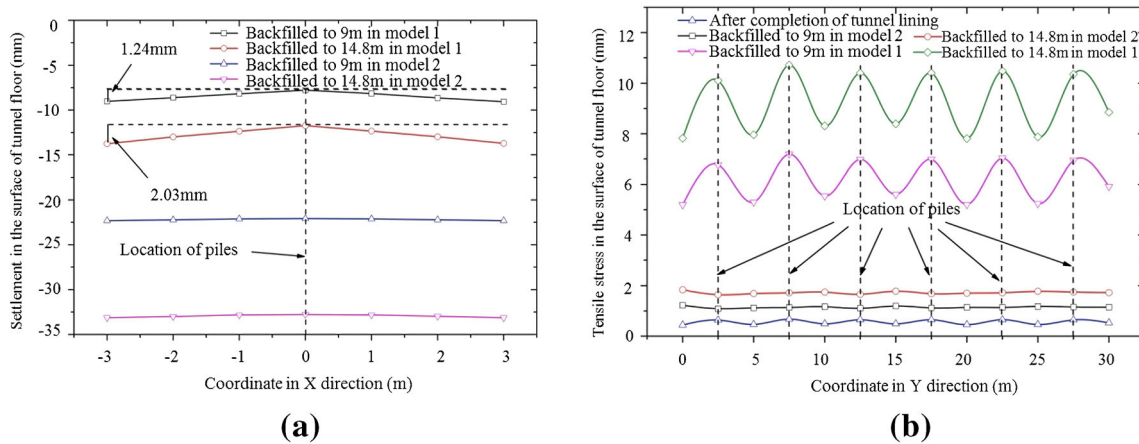


Fig. 11 Numeric results comparison of model 1 and model 2. (a) Settlement along line B-B' (b) Tensile stress along line B-B'

concrete, but the settlement is large, leading to uneven settlement along the longitudinal direction. In model 1, the deformation pattern of the tunnel floor is similar to a cantilever, which makes tensile stress in tunnel model 1 distribute unevenly and dramatically exceeds the ultimate tensile strength of concrete. It can be inferred that uneven settlement is the immediate cause of damage zones, but the primary cause is the significant stiffness difference between bored piles and SRM.

Figure 12 shows the settlement of models 1 and 3 along line B-B'. Settlements in models 1 and 3 are identical when backfilling to 9 m. The maximum settlement was 9.05 mm and the maximum uneven settlement of was 1.24 mm, since reinforcement measures were taken when backfilling to 9 m. Settlement in models 1 and 3 both increased with the height of backfill. When backfilling to 14.8 m, the maximum settlement and uneven settlement of model 1 increased to 13.72 and 2.03 mm. The maximum settlement and uneven settlement values of model 3 increased to 11.23 1.40 mm, respectively. The

settlement and uneven settlement of model 3 are less than model 1, which means that uneven settlement can be well controlled.

Figure 13 shows the distribution of damage zones and tensile stress on the tunnel floor. The width and thickness of the damage zones are 2.4 and 0.6 m, respectively. About 40% of the tunnel floor will be tensioned to damage in model 3. The damage zones in model 3 are less than model 1. The tensile stress distribution in model 1 and 3 is similar when backfilling to 14.8 m. However, the tensile stress in model 3 is much less than model 1, which means the suggested reinforcement measures are effective in improving stress distribution on the tunnel floor. The maximum tensile stress on the fiber-reinforced concrete's surface is 2.89 MPa, which is within the ultimate tensile strength of fiber-reinforced concrete. The steel fiber-reinforced concrete method was necessary to ensure that tensile stress in the tunnel floor falls within the ultimate tensile stress of concrete. Based on the development of settlement

Fig. 12 Settlement along line B-B' in model 1 and 3

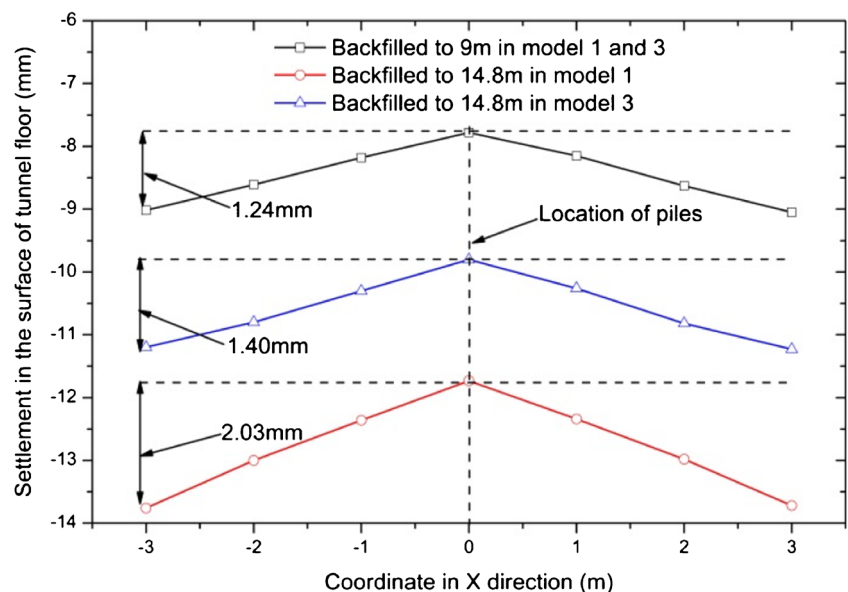
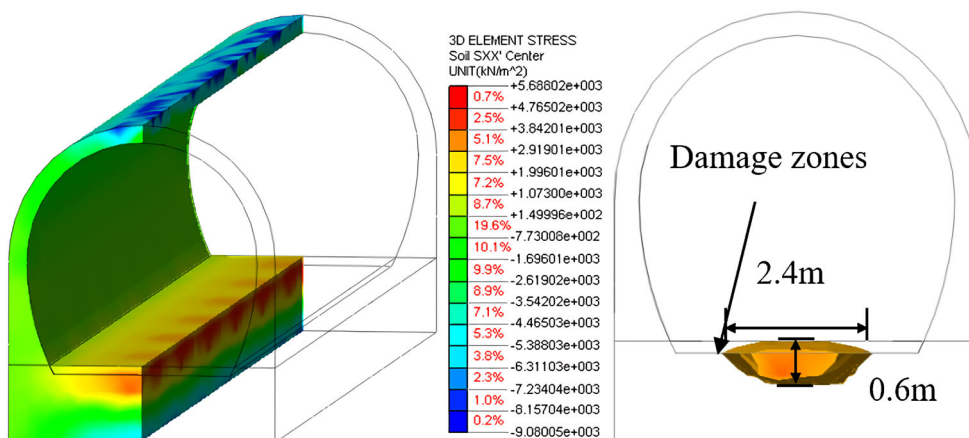
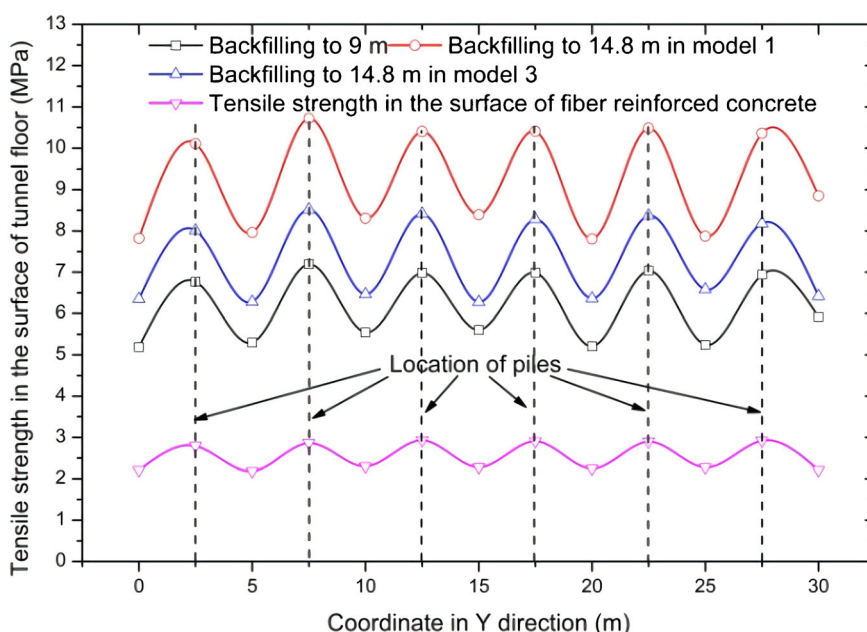


Fig. 13 Distribution of damage zones and tensile stress in model 3 when backfilling to 14.8 m. **(a)** Damage zones, **(b)** Tensile stress



(a)



(b)

and tensile stress in the tunnel floor, it can be summed that these two suggested reinforcement measures are effective in improving stress distribution and damage resistance of tunnel lining.

Discussion

The mechanisms of suggested reinforcement measures

In the view of designers, bored piles were designed to improve the bearing capacity of SRM and further decrease tunnel settlement. Unfortunately, severe longitudinal cracks appeared in the tunnel floor when backfilling to 9

m above the tunnel. Three comprehensive 3D numeric models were established. The results were analyzed and compared to investigate the development and causes of damage zones in the tunnel lining. Settlement and tensile stress distribution on the tunnel floor were highlighted. Through comparing the results of construction steps 2 and 3 in model 1, approximately 66% of the tunnel floor will be damaged if no reinforcement measures were taken. Reinforcement measures must be adopted to prevent the significant development of damage zones on the tunnel floor. Causes of tunnel lining damage were investigated by comparing the results of models 1 and 2. Results show that the settlement of model 1 is not uniform but is much lower than that of model 2. However, the tensile stress in model 1 is not uniform but is much larger than in model 2.

Due to bored piles, settlement above bored piles is much less, but tensile stress is much larger than model 2 without bored piles. In engineering practice, the tunnel floor's deformation and stress pattern are similar to that of a cantilever (Fig. 14). The gravity of the SRM above the tunnel lining is firstly transferred to the tunnel floor and then to the foundation. Bored piles support the middle part of the tunnel floor, and SRM supports the other tunnel parts. Generally, the elastic modulus and stiffness of bored piles are much larger than SRM. The subgrade reaction provided by the SRM is much lower than the bored piles, which will result in uneven settlement. Based on structural mechanics theory, the bored piles can be considered rigid fixing support compared to SRM. The maximum bending moment occurred on the tunnel floor above bored piles. The upper part of the tunnel floor will be tensioned, and the lower part will be compressed, which will result in the appearance of damage zones in the tunnel lining. The mechanical characteristic of model 2, the bored piles were removed, the subgrade reaction distributes uniformly in the tunnel floor. The tunnel lining will deform entirely. When SRM below the tunnel lining was reinforced through grouting, the subgrade reaction provided by SRM will have a more significant increase than without taking reinforcement measures. As a result, the bending moment in the tunnel floor will be much lower than without reinforcement measures (Fig. 14). The grouting method can well control the development of damage zones on the tunnel floor.

The innovation and shorting coming of research

In this paper, the causes of damage zones in a tunnel constructed in SRM were identified, and the effectiveness of corresponding reinforcement measures was evaluated. The suggested reinforcement measures, including sleeve grouting and fiber-reinforced concrete, can effectively control the development of the settlement, uneven settlement, tensile stress, and the damage zones. These two reinforcement measures can be taken in future similar engineering situations. The research results can provide a theoretical basis for the construction and reinforcement of tunnels located in the SRM foundation.

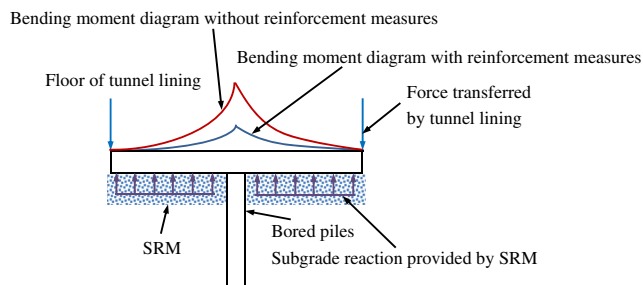


Fig. 14 Force and bending moment diagram on the tunnel floor

However, it is a complex problem to study the stability of the tunnel structure on the SRM foundation, and the crack of the tunnel lining is also the difficulty of the quality control of the tunnel engineering. There are several deficiencies in this study. Firstly, due to the limitation of time and site conditions, the mechanical test of the SRM fill foundation cannot be carried out, and the related mechanical test can be carried out in later research. Secondly, the influence of the SRM foundation's consolidation on the stability of the tunnel structure has not been considered. Thus, the consolidation of the SRM foundation should be taken into consideration in a further study.

Conclusion

This paper focuses on identifying the causes of damage zones in the tunnel lining when constructing in SRM. The physical and mechanical parameters of SRM were firstly obtained by conducting numerical modeling experiments. Three comprehensive numeric models were established based on three working conditions. The settlement and stress distribution in the tunnel were highlighted to identify the development trends and causes of damage zones and evaluate the effect of suggested controlling the development of damage zones.

If no reinforcement measures are taken, about 66% of the tunnel floor will be tensioned to damage, significantly reducing the bearing capacity and long-term stability of tunnel lining. To avoid severe damage to the tunnel, only if reinforcement measures are taken to control the development of damage zones backfilling can be continued.

The significant stiffness difference between SRM and the bored piles is the reason for damage zones in tunnel lining. The deformation pattern of the tunnel floor is similar to a cantilever. The maximum bending moment occurred in the center part of the tunnel floor.

When the tunnel is constructed in SRM, it is suggested that grouting reinforcement or support beams at the bottom of the tunnel lining should be combined with bored piles to improve the bearing capacity of foundations. Besides, steel fiber-reinforced concrete is suggested to be cast on the tunnel floor to improve damage resistance.

Acknowledgements This research is funded by the National Natural Science Foundation of China (No. 51578091). The financial support from the NSFC is much appreciated.

Declarations

Conflict of interest The authors declare that they have no conflict of interest in this work.

References

- Chiaia B, Fantilli AP, Vallini P (2009) Combining fiber-reinforced concrete with traditional reinforcement in tunnel linings. *Eng Struct* 31(7):1600–1606. <https://doi.org/10.1016/j.engstruct.2009.02.037>
- China Merchants Chongqing Communications Technology Research & Design Institute CO LTD (2010) Code for Design of Road Tunnel. China Communications Press, Beijing
- Cui BW (2012) Study on deformation characteristics of expansive soft rock tunnel in fault zone. Chongqing University
- Dalian University of Technology (2004) Technical specification for fiber reinforced concrete structures. China Architecture & Building Press, Beijing
- Fakhimi A (2009) A hybrid discrete–finite element model for numerical simulation of geomaterials. *Comput Geotech* 36(3):386–395. <https://doi.org/10.1016/j.compgeo.2008.05.004>
- Lee CH, Chiu YC, Wang TT, Huang TH (2013) Application and validation of simple image-mosaic technology for interpreting cracks on tunnel lining. *Tunn Undergr Space Technol* 34:61–72. <https://doi.org/10.1016/j.tust.2012.11.002>
- Li X, Liao QL, He JM (2004) In-situ tests and a stochastic structural model of rock and soil aggregate in the three gorges reservoir area, china. *Int J Rock Mech Min Sci* 41(3):702–707. <https://doi.org/10.1016/j.ijrmms.2004.03.122>
- Mashimo H, Isago N, Kitani T, Endou T (2006) Effect of fiber reinforced concrete on shrinkage crack of tunnel lining. *Tunn Undergr Space Technol* 21:382–383
- Research Institute of Highway Ministry of Transport (2007) Test Methods of Soils for Highway Engineering. China Communications Press, Beijing
- Richards JA (1998) Inspection, maintenance and repair of tunnels: international lessons and practice. *Tunn Undergr Space Technol* 13(4): 369–375. [https://doi.org/10.1016/S0886-7798\(98\)00079-0](https://doi.org/10.1016/S0886-7798(98)00079-0)
- Sun SR, Xu PL, Wu JM et al (2014) Strength parameter identification and application of soil–rock mixture for steep-walled talus slopes in southwestern China. *Bull Eng Geol Environ* 73(1):123–140. <https://doi.org/10.1007/s10064-013-0524-1>
- Vallejo LE, Mawby R (2000) Porosity influence on the shear strength of granular material–clay mixtures. *Eng Geol* 58(2):125–136. [https://doi.org/10.1016/S0013-7952\(00\)00051-X](https://doi.org/10.1016/S0013-7952(00)00051-X)
- Wang XL (2009) Study on comprehensive evaluation technology of underground grouting effect. Beijing Municipal Engineering Research Institute
- Wang TT (2010) Characterizing crack patterns on tunnel linings associated with shear deformation induced by instability of neighboring slopes. *Eng Geol* 115(1-2):80–95. <https://doi.org/10.1016/j.enggeo.2010.06.010>
- Wang Z, Wang LZ, Li LL, Wang JC (2014) Failure mechanism of tunnel lining joints and bolts with uneven longitudinal ground settlement. *Tunn Undergr Space Technol* 40:300–308. <https://doi.org/10.1016/j.tust.2013.10.007>
- Xiao JZ, Dai FC, Wei YQ, Min H, Xu C, Tu XB, Wang ML (2014) Cracking mechanism of secondary lining for a shallow and asymmetrically-loaded tunnel in loose deposits. *Tunn Undergr Space Technol* 43:232–240. <https://doi.org/10.1016/j.tust.2014.05.013>
- Xu WJ, Hu RL, Tan RJ (2007) Some geomechanical properties of soil–rock mixtures in the Hutiao Gorge area, China. *Geotechnique* 57(3): 255–264. <https://doi.org/10.1680/geot.2007.57.3.255>
- Xu WJ, Xu Q, Hu RL (2011) Study on the shear strength of soil–rock mixture by large scale direct shear test. *Int J Rock Mech Min Sci* 48(8):1235–1247. <https://doi.org/10.1016/j.ijrmms.2011.09.018>
- Xu WJ, Yue ZQ, Hu RL (2008) Study on the mesostructure and mesomechanical characteristics of the soil–rock mixture using digital image processing based finite element method. *Int J Rock Mech Min Sci* 45(5):749–762. <https://doi.org/10.1016/j.ijrmms.2007.09.003>
- Yue ZQ, Chen S, Tham LG (2003) Finite element modeling of geomaterials using digital image processing. *Comput Geotech* 30(5):375–397. [https://doi.org/10.1016/S0266-352X\(03\)00015-6](https://doi.org/10.1016/S0266-352X(03)00015-6)
- Zhang DP (2010) Application of grouting technology in subway tunnel in saturated silty fine sand stratum. China University of Geosciences, Beijing
- Zhao Y, Liu Z (2019) Numerical experiments on triaxial compression strength of soil–rock mixture. *Adv Civ Eng* 2019(Pt.2):1–15